COMPARISON OF INJURY PREDICTORS AND KINEMATICS OF HUMAN BODY MODELS REPRESENTING AVERAGE FEMALE AND MALE ROAD USERS IN CAR CRASHES

Corina Klug, Felix Ressi, Christoph Leo
Vehicle Safety Institute
Graz University of Technology
Austria

Michal Kowalik, Ines Levallois
Forvia Automotive Seating,
Poland/France

Johan Iraeus, Jobin John, I Putu A. Putra, Mats Svensson
Vehicle Safety Division
Sweden

Astrid Linder
VTI - Swedish National Road and Transport Research Institute; Chalmers University of Technology
Sweden

Arne Keller, Linus Trummler, Kai-Uwe Schmitt
Arbeitsgruppe für Unfallmechanik (AGU Zürich)
Switzerland

Paper Number 23-0133

ABSTRACT

Differences in injury risk between females and males are often reported in field data analysis. The aim of this study was to investigate the differences in kinematics and injury risk between average female and male car occupants, pedestrians and cyclists, under well-controlled boundary conditions. Therefore, a simulation study comprising the newly introduced VIVA+ human body models was performed, representing the first model line-up consisting of average female and male models originating from the same base model. A generic vehicle interior, detailed seat models and a generic vehicle exterior were used to simulate crash scenarios close to those currently tested in consumer information tests. Differences in injury risks, load distribution and injury mechanisms were observed between the average female and male VIVA+ models for different load cases and body regions. While in some load cases, loading was more severe for the average female, opposite trends have also been observed. In order to understand trends observed in the field and to derive appropriate countermeasures, further variations in load cases and anthropometries should be considered in future work using the tools presented in this study.

INTRODUCTION

Although vehicle safety systems have improved over the past few decades, several studies show that women and men are not equally protected [1]. A comparison of the risk of injury between males and females reveals that females are exposed to higher injury risks among a range of different crash types [1–5]. Females have a higher risk of injury to the lower extremities [6], torso, and cervical spine [3], than males, while males show higher risks for skull fractures and severe brain injuries in frontal impacts [3]. Especially, higher risks for females have been identified with regard to the risk of injury involving long-term consequences [1]. When filtered to similar vehicle types, differences in odds ceased to be significant in frontal and side crashes for non-extremity injuries, but remained for MAIS2+, especially for extremity injuries [6]. The reasons for such differences are complex and manifold.

Nutbeam et al. [5] investigated differences between women and men with regard to the probability of entrapment, frequency of injury and outcome, following a motor vehicle collision. The results show that female patients were significantly more frequently trapped than male patients. Trapped male patients suffered head, face, thoracic and limb injuries more frequently, while female patients had sustained more injuries to the pelvis and spine. [5]

Gender- and age-specific differences in injury patterns were also observed in Vulnerable Road User (VRU) crashes, revealing also that some crash types (especially on rural roads) are more likely to occur for males than for females, further complicating comparisons [7].

Comparability between different cases is an issue always present in accident analysis. When too many filters are applied or variables considered, case numbers decrease rapidly, especially in Europe, where in-depth data is still limited. Differences in injury protection between the female and male sub-populations cannot be detected in regulatory tests since it is the average male (50M) that is predominantly studied in vehicle safety assessments [8]. Currently, beside the 50M, crash test dummies representing the 5th percentile female (05F) and 95th percentile male (95M) are available, but none representing the average female part of the population. In the study by Schneider et al. [9], defining the target anthropometry of current crash test dummies, in addition to the three previously mentioned dummy statures, designing a mid-sized female (50F) was also recommended. However, due to funding constraints, the 50F anthropometry was dropped and current dummy families still only comprise a

maximum of three statures. To date, no standardised crash test dummy representing the 50F anthropometry is available and is thus not used in regulations or consumer information tests.
The implementation of virtual testing using Human Body Models (HBMs) has facilitated more detailed consideration of anthropometric differences than general crash test dummies. The advantage of simulation studies is the ability to study differences in well-controlled boundary conditions. An objective comparison between average male and average female injury risks requires models with a sufficiently comparable modelling approach, which has not been available so far. The recent development of the VIVA+ models, however, gives an opportunity to compare male and female responses using equivalent models.
The aim of the current study was to investigate the differences in kinematics and injury risk between average females and males in load cases close to current consumer information safety testing. The focus of these investigations was on car occupants and VRUs utilising the novel VIVA+ 50M and 50F models.

METHOD

The open-source VIVA+ 50F and 50M HBMs (version 0.3.2)[1], which were previously validated on component and full-scale levels [10–12], were used in this study. The 50M and the standing models differ from the baseline, the seated 50th percentile female (50F) model only in terms of geometry and mass distribution. The template meshes for the average female and male, consisting of the outer skin and surfaces of all skeletal parts was obtained from statistical shape models [10]. All derivative models (the standing 50F, and the seated and standing 50M) were generated via a custom morphing code to match the landmarks of the template meshes on the bones and outer shape [10]. All contacts, material models and element formulations are the same among all derivative models, enabling a novel way of comparing the response of the average female and male based on differences in anthropometry only. Simulations were performed in LS-Dyna R12.0 (VRU), or R9.3.1 (occupant simulations).
The kinematics and injury risk of the 50F and 50M VIVA+ models have been compared for the following crash scenarios:

- Car occupant in frontal impact
- Car occupant in near-side impact
- Car occupant in rear end impact
- Pedestrian impacted by a car
- Cyclist impacted by a car

Simulation Setups

Frontal and Near-Side Impacts

For the frontal and side impacts, a previously published generic vehicle interior (GVI) was used [13]. The VIVA+ models were positioned according to the regression models from Park et al. [14] into a pre-deformed seat. An overlay showing both models is presented in Figure 1.

Figure 1. Comparison of the final postures of the 50F (orange) and the 50M (blue). Note that the same eye level was achieved and both occupants can reach the pedals as well as the steering wheel.

Generic crash pulses were applied in both load cases. For the frontal load case, two generic previously published pulses [15] were selected. Specifically, a full-frontal impact at 56 km/h (Δv=65.6 km/h) and an oblique impact (initial velocity of host and opponent at 53 and 35 km/h and an impact angle of 4° and -21°, respectively, resultant Δv=53 km/h). For the lateral load cases, the generic crash pulse (Δv=32 km/h) previously used by [16] with the same GVI model was used with two different maximum intrusions. The restraint system parameters were varied

[1] https://vivaplus.readthedocs.io

to mimic different vehicles. Details of the simulation matrix resulting in 27 frontal and 6 side crashes for each occupant model (66 simulations in total), are presented in Table A2 and Table A4 in Appendix A1.

Rear Impacts

Simulations with the VIVA+ model version 0.2.4 in a conceptual Forvia innovative seat (Figure 2) with integrated retractor have been performed with three different headrest positions (uppermost, lowermost and mid-position).

Figure 2. Conceptual orvia innovation seat used for rear impact simulations

The HBM was positioned on the seat according to the regression model presented by Park et al. [14] within the first 300 ms of the simulation before the crash pulse was applied allowing the body to adjust to the seat during the settling. The pulses were applied by prescribed motion. No seatbelt was used in the rear end simulations as previous studies have shown that this has negligible effect during the early phase [17], which was of most interest for the current study.

VRU Load Cases

For the VRU impacts, two generic vehicle exteriors (GVE) representing a Sedan and an SUV shape were used for simulation of collisions at 40 km/h. Revision 3 of the official CoHerent (Euro NCAP Technical Bulletin 024) Generic Vehicle models, where a deformable windshield was included. The stiffness of the different parts of the GVE were re-evaluated, comparing them with data available from literature regarding different stiffness levels of the current European fleet. The results of the impactor tests can be found in Table A5 and Figure A5 in Appendix A2. The standing VIVA+ models were positioned in a pedestrian stance in accordance with the specifications of the Euro NCAP TB024. For the cyclist simulations, the 50M and 50F cyclist models were positioned on different bicycles to meet realistic cycling postures. Further specifications on the bicycle models and the positioned cyclist models can be found in Appendix A2. The cyclist and pedestrian were impacted at the vehicle centreline of both vehicle shapes and oriented relative to the vehicle once at 90° and once at 270°.

Outputs

The LS-Dyna output (binout) files were post-processed using the Python library Dynasaur. In the rear impact simulations, the rotation of each vertebrae Centre of Gravity (CoG) around the global y-axis, the head and T1 accelerations and the Neck Injury Criterion (NIC), were analysed. For the other load cases, kinematic head injury assessment (Head Injury Criterion (HIC), DAMAGE), strain-based rib fracture assessment (risk of 3+ fractured ribs) and strain-based lower extremity fracture assessment (risk of proximal and femur shaft fracture) have been calculated. More detailed documentation of the applied injury risk functions is available in Table A1. For body regions where risk curves are still under development, the 99th percentile maximum principal strains (99MPS) were evaluated.

RESULTS

In the following chapter, results of the simulations with the 50F and 50M for the different load cases are presented in a short format. More detailed results are available in Appendices B1 - B3.

Frontal Impacts

The scatter plot in Figure 3 illustrates the differences in injury risk for the two models by representing each injury criterion as a symbol, with the injury risk of the 50M on the horizontal axis and the injury risk for the 50F on the vertical axis, for each simulation. The three colours represent the three load cases (FF56, ONS, and OFS) which were used in the simulations. The parameters for the individual simulations are provided in Table A2 and the respective results are provided in Table B1.

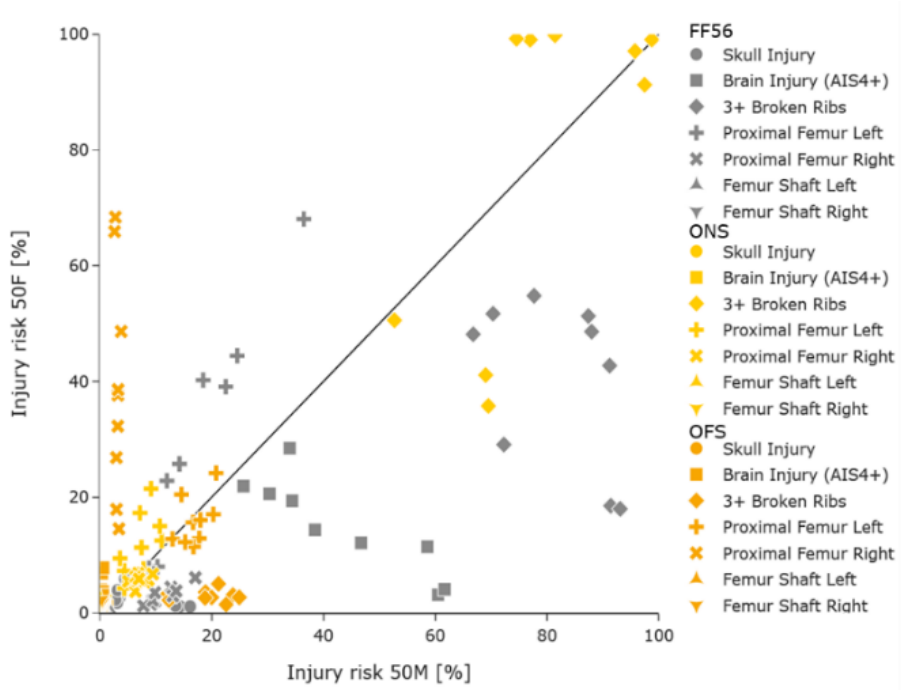

Figure 3. Scatter plot illustrating the injury risk of the 50M (horizontal axis) and the 50F (vertical axis) for the 27 frontal/oblique load cases performed with each anthropometry. In cases below the diagonal line, higher injury risk was observed for the 50M and in cases above, higher injury risk was observed in the 50F. The grey symbols represent the FF56 load cases, the yellow symbols ONS and the orange symbols OFS load cases.

At a glance, Figure 3 illustrates that the injury risk for different body regions can vary considerably between the two models and the three load cases. In some cases, the injury risks were low for both models (i.e., brain injury in the oblique load cases) and in some, the injury risk, while increased, was similar for both anthropometries, close to the diagonal line, (i.e., the proximal left femur injury risk for the majority of oblique cases). However, there were a number of cases with large injury risk deviations between the 50F and 50M. The risk of injury to the right proximal femur in the OFS load case (orange 'x' in Figure 3) is below 5% in all variants for the 50M. In contrast, for the same parameters, the risk for the 50F varies from 15-68%. For the FF56 load case, the risk of injury to the left proximal femur (grey cross in Figure 1) almost seems to follow a linear relationship, with the 50F experiencing higher injury risk (for higher knee bolster stiffness levels) in most cases. A different relationship was observed for brain injury risk in the FF56 load case (grey squares in Figure 3). For the lowest airbag pressure levels, the risks are similar for the two models (between 22% and 34%). However, with increased airbag pressures, the risk for the 50F decreased while the risk for the 50M increased. The risk of three or more rib fractures (diamond symbols in Figure 3) varied considerable with both, load case and anthropometry. The risk was lowest in the OFS load case, where the risk for the 50F was 5% or less, while for the 50M the risk varied between 12% and 25%. In the FF56 load case, the risk was highest for the 50M (93%) with the softest airbag/belt setting, which yielded the lowest injury risks for the 50F (18%). Again, increasing the airbag and belt stiffness reduces the risk for the 50M and increases the risk for the 50F. In the ONS load case, the risk for three or more fractured ribs (yellow diamonds in Figure 3) was lowest for both models with the softer airbag and belt setup (50F: 36%, 50M: 53%). In all cases with the increased stiffness, the injury risk was above 90% for both models and for the mean stiffness settings, the 50F was above 99% while the 50M was at less than 82%.

Side Impacts

In the six simulated near-side impacts, differences between the models varied for the considered injury predictors. Like for the frontal load cases, a scatter plot (Figure 4) illustrates these differences. The two colours represent the two intrusion levels that were applied in the simulations. Since most criteria form relatively tight groups, the three side airbag (SAB) pressure levels that were used are not differentiated in the plot. The triangles in the bottom left corner indicate that the risk of femur shaft injury was very low for both anthropometries. Skull fracture risk was higher for the 50F in all cases while the brain injury risk was increased for the average male, particularly for the load cases in which the larger maximum intrusion was applied. Proximal femur injury risk was higher for the 50M. Finally, the risk of three or more fractured ribs was more ambiguous. For the mean intrusion level, the 50M predicted the higher risks. For the larger intrusion level, the results vary depending on the SAB pressure. For the lowest pressure level, both models predicted similar risks at about 50%. For the two other pressure levels, the risk for the average male is very similar at around 8%, while for the 50F risks of 28% (higher pressure level) and 46%

(mean SAB pressure level) were observed. All input parameters are listed in Table A4 and the complete results are presented in Table B2.

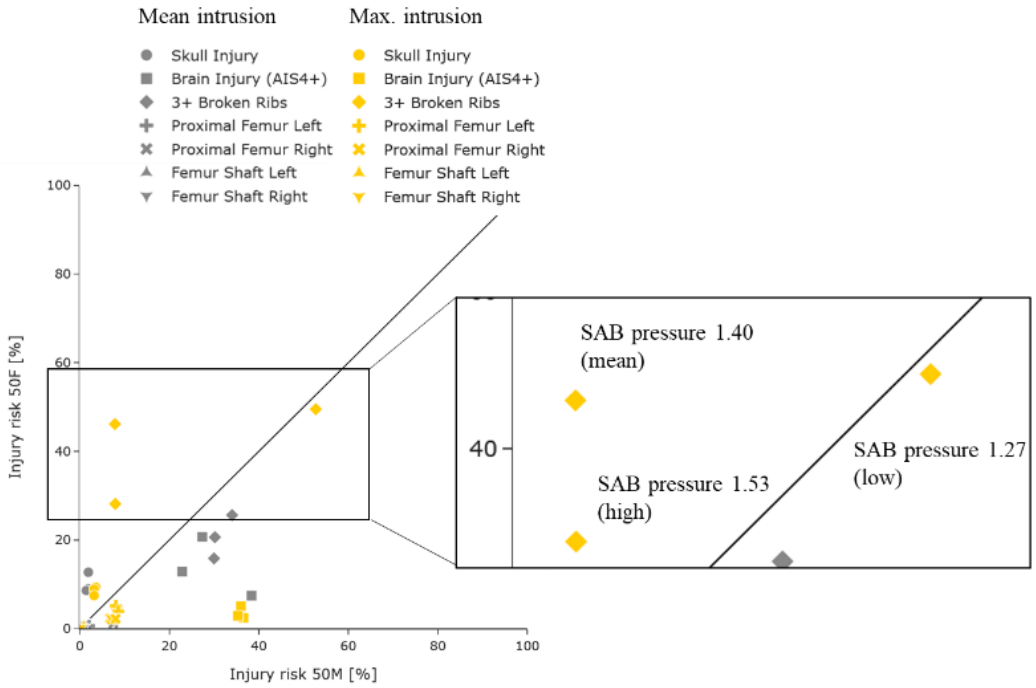

Figure 4. Scatter plot illustrating the injury risk of the 50M (horizontal axis) and the 50F (vertical axis) for the six side impact load cases performed with each anthropometry. In cases below the diagonal line, higher injury risk was observed for the 50M and in cases above, higher injury risk was observed in the 50F.

Rear Impacts

An overview on the simulation results are shown in Table 1. The NIC was higher for the 50F in all simulations with the highest value for the uppermost headrest position.

Table 1.
Results of rear impact simulations.

	NIC [m^2/s^2]	
Headrest position	50M	50F
uppermost	13.3	22.9
mid-position	6.9	19.5
lowermost	11	15.4

The detailed analysis of kinematics (Figure 5) shows the movement pattern of the 50F compared to the 50M in the seat with uppermost headrest position.

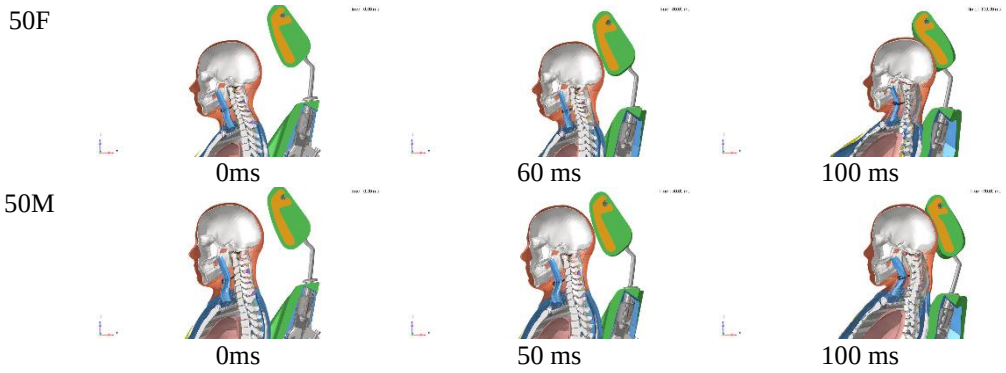

Figure 5. Kinematic of the VIVA+ 50F and 50M with uppermost headrest position

VRU Impacts

The results of the pedestrian and cyclist simulations for the different body regions, initial orientations and vehicle shapes are summarised in Figure 6. All results of the individual simulations are shown in Table B4 for the pedestrian and Table B5 for the cyclist.

For the pedestrian, HIC and DAMAGE values were higher for the SUV than for the Sedan, consistent for 50M and 50F. The risk of more than three fractured ribs was considerably higher for the 50F compared to the 50M in all load cases, except for the 90° Sedan load case, where no contact between vehicle and chest was observed for the female (see Figure B7), and therefore the risk was close to 0. The proximal femur fracture risk of the struck side leg was very high for the female in all load cases (89-100%), while it was only 6-13% for the male for the Sedan load cases, but 100% for the SUV load cases. The risk for femur shaft fractures was similar for both anthropometries, being higher in the Sedan load cases than the SUV cases.

For the cyclist, HIC values were again mainly depending on the vehicle shape, but were lower for the Sedan than for the SUV. For the SUV 90° impact, the skull fracture risk based on HIC was twice as high for the 50M than for the 50F. The risk of more than three fractured ribs was higher or equal for the 50M in the Sedan load cases, while being higher for the 50F in the SUV load cases. The risk for proximal femur fractures was higher for the 50F in all load cases except for the Sedan 270° where both risks were very similar (13% for 50F and 16% for 50M). The femur shaft fracture risk was higher than for the 50M except for the SUV load case at 270°, where risks were again equally high (85% for 50F and 97% for 50M).

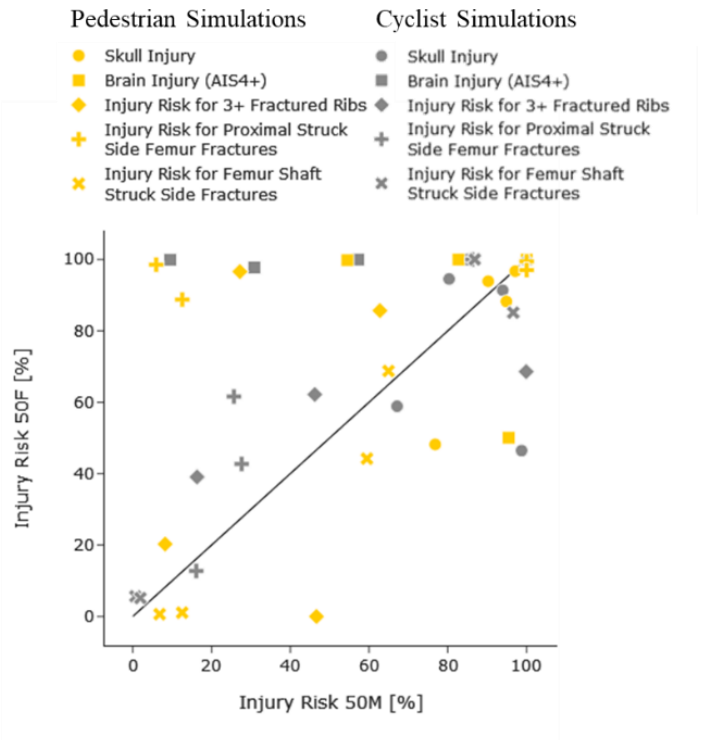

Figure 6. Summary of cyclist and pedestrian simulation results for 50F and 50M for different body regions.

DISCUSSION

Overall, trends in predicted injury risk between females and males were different in different load cases and in different body regions. In some of cases or body regions, the 50M was at higher risk and sometimes the 50F.

Frontal and Side Impacts

In an effort to mimic different vehicles while using a single generic vehicle interior, restraint system parameters were varied. Although four load cases (full frontal, oblique near-side, oblique far-side and lateral near-side) were considered, the simulation results cannot be compared to field data directly. However, the results enable a broader perspective compared to single load case analyses.

For the frontal load cases, it was observed that restraint system adaptations favourable for the male are not necessarily improving the performance for the female. For instance, the rib fracture risk is reduced for the 50M when increasing the airbag and seatbelt load limiter stiffness, while these adaptions increase the risk for the 50F. Also opposite trends were observed with higher risks for the male indicating that adaptive restraints might be already benefititial between the 50M and 50 F stature. While such adaptive restraint systems are often discussed for optimising the pvonerformance between the average male and small female, the results presented above indicate that they would also be beneficial for the average female, which is far more similar in anthropometry to the average male than the small female.

The average female showed higher injury risks for the lower extremities compared to the 50M, which is in line with field data [6].

Furthermore, differences in belt interaction (see Appendix B1) causing load distribution differences within the chest were also observed between the 50F and 50M. In the present study, identical restraint system settings were assumed for the female and male. While it is common that airbag and seatbelt parameters are adapted between the 05F and 50M, this is unlikely for the 50F, as this size is currently not assessed in regulations or consumer information safety assessments.

The injury risk for near-side collisions is highly affected by the location of the intrusions. While an average intrusion pattern (see Appendix A1.2) was applied, it was identical for both models. Compared to the frontal and oblique simulations, the maximum injury risks were lower in the near-side collisions. Although the generic side and curtain airbag in the GVI did protect both, the 50M and 50F well, differences were still observed. Skull fracture injury risk was below 4% for the 50M in all cases, and injury risks between 9-13% were obtained for the 50F. This was due to the shape of the generic curtain airbag, which provided less protection at the 50F head position. While this might not be an issue with modern vehicles and robust curtain airbag geometries, it still highlights the importance of providing adequate airbag depth for different anthropometries in various seat adjustments. Similarly, the higher brain injury risks for the 50M can be explained by the way the head interacts with the curtain airbag.

The largest injury risk differences in the near-side simulations were observed for the ribs. In the cases where the mean intrusion level was applied, the risk for three or more fractured ribs was higher for the 50M. While similar for the mean and higher SAB pressure level, it was considerable higher for the 50M (38%) with the softer pressure level, which in turn produced the lowest risk for the 50F (7%). When the maximum intrusion level was applied, this softer setting produced the highest risks for both models (approx. 50%). However, with the maximum intrusion applied, both alternative SAB pressure settings produced low risks for the 50M (8%), while for the 50F, these settings resulted in risks between 28% and 46%. The main reason for this was that the 50F model interacted with the door trim differently, resulting in bending of the 12th left rib, which did not occur for the 50M. While the extent of this difference in injury risk will be dependent on the intrusion pattern and the individual vehicle, it highlights that using an additional anthropometry can help uncover designs, which potentially increase the injury risk for some anthropometries and postures.

While in conventional pole impact crash tests, the pole is always aligned with the occupant's head CoG, in the present study, the same intrusion pattern was applied to both models. However, since this study focused on comparing the model responses under identical load conditions, the presented approach was deemed more suitable.

Rear Impacts

The major challenge in the analysis of the rear impact cases was the question of a significant injury predictor of whiplash injuries to the neck. Analysing the NIC only, it appeared that some of the observed mechanisms were missed. NIC was designed to predict potential nerve injury causing pressure transients in the vertebral canal, presented by [18], here denoted Aldman pressure. An observed compression of the cervical spine is expected to be related to the injury mechanism focusing on the strains in the facet joints, which have not been considered in the current study. In a previous study by Kitagawa et al. [19], higher first peaks of strains in the joint capsule were observed for simulations with a 50F HBM compared to a 50M HBM. In the field, a combination of injury mechanisms might be present, which is currently not reflected by any injury predictor and should be considered in future research.

As the threshold for NIC is not comparable between females and males due to differences in the spinal canal, it would need to be adapted [20]. Schmitt et al. [20] suggested a threshold for risk of injury of 12 for the average female, compared to 15 for the male.
Based on the results with the Forvia innovative seat, setting the headrest position excessively high could be one possible reason for higher injury risks for females in the field. Integrated head restraints could potentially solve this issue, however, consideration of different statures is required when developing the inner structure of such head restraints to avoid unfavourable loading for smaller or taller occupants than the 50M.

VRU Impacts

Two generic vehicle models (generic Sedan and SUV) were used in the VRU crashes. Although they were tuned to simulate a representative stiffness, the models are still more simplified and homogeneous than a real car would be. In addition, the windshield model is rather simplified compared to windshield models used in finite element (FE) models of serial cars.
Furthermore, for the VRU crashes only one initial (walking or cycling) posture was simulated and analysed in the current study and only two different orientations (perpendicular to the vehicle with either left or right leg as struck-side). The higher proximal femur fracture risk observed in the simulations with the 50F was caused by the different impact locations of the bonnet leading edge on the femur due to the different stature, which is shown in Figure B7. A higher risk for lower extremity injuries for females was also observed in the field and therefore seems plausible [7]. Current development of leg form impactors mainly focuses on the stature of the average male. Based on the current results, simulations with smaller statures might be beneficial and should be considered when evaluating the upper leg form impactor tests.
For the cyclist simulations, different initial positions of the cyclist 50F and 50M have intentionally been selected, as it was decided that it would be most meaningful to adopt different initial positions based on the most common female and male bicycles, rather than using the same bicycle for both. However, this approach may affect the results, as the head injury risk, for instance, is highly affected by the impact location.
In general, injury predictions for the VRU cases seem to be relatively high. This could be due to the applied injury risk curves, which are often based on tests with subjects biased towards higher age. Another possible cause could be the stiffness of the GVE, which is an "averaged" stiffness that does not represent a specific production car and could lead to some unrealistic behaviour overall.

Limitations

Sex-related differences in material properties were not considered on the tissue level in the VIVA+ models. Material properties represent the average values reported in literature, which does not necessarily correspond to the target age of 50 years due to the bias towards elderly donors.
The 50F and 50M anthropometries are based on regression models representing an average fifty-year-old female and male, which were selected to represent the average age of the injured adult population involved in car crashes. However, in the field we can see peaks for the younger and the older population and higher differences in female and male injury risks for younger occupants. Variability within the anthropometry of females and males has not been taken into account in this study, but should be further investigated in the future.
The VIVA+ models were validated for a wide range of load cases. However, in the validations often considerable scatter is observed within experiments. Furthermore, not all body regions were in focus of the VIRTUAL project, which is why for example submarining prediction or upper extremities have not been validated so far.
Furthermore, the lack of validated injury risk curves for HBMs is another limitation, especially for rear impacts, as discussed in the previous section. In addition, the same injury risk curves have been applied for the 50F and 50M, although sex-specific injury risk curves might be required for the kinematic injury metrics used (NIC, DAMAGE, HIC), which requires sufficient data for calibration.
Another limitation in all performed occupant simulations is the definition of comparable seating positions and resulting postures between the 50F and 50M. We have endeavoured to find a compromise in this study between defining comparable positions between the 50F and 50M, and positions that are realistic for both, as they are based on regression models from volunteer studies. This, however, could also be one of the major contributory factors in different injury risks.
As the current study focused on the simulation of load cases similar to standardised tests without variations of extrinsic and intrinsic factors present in real-world crashes, no meaningful comparison with field data was possible.

Future Work

In the future, additional load cases in a variety of initial positions and postures should be investigated. Doing that, the tools introduced in the current study could be used in larger simulation campaigns allowing comparison with field data. This would enable the identification of the main contributing factors for the differences in injury risks between females and males, and finally help derive appropriate countermeasures.

CONCLUSIONS

In all load cases, differences in kinematics, loading patterns and injury mechanisms were observed. Based on the current study, it cannot be confirmed that the 50M and 50F always behave similarly, or that the 50M represents the worst-case in general. It is recommended to further investigate the behaviour of the 50F in future studies since it represents a large portion of the population. Due to the opportunity of virtual testing, even more anthropometries (i.e., models representing obese or elderly individuals) should be considered in the future to cover a wider range of the population and make sure that vehicle systems robustly protect every person in the population involved in vehicle crashes.

ACKNOWLEDGEMENTS

This study was conducted within the VIRTUAL project, funded by the European Union Horizon 2020 Research and Innovation Programme under Grant Agreement No. 768960. Language review was performed by Elisabet Agar.

REFERENCES

[1] Kullgren, A., Stigson, H., and Axelsson, A., "Developments in car crash safety since the 1980s," in: International Research Council on the Biomechanics of Injury (ed.), *2020 IRCOBI Conference Proceedings*, IRCOBI Conference Proceedings, IRCOBI Conference, postponed (online), IRCOBI, ISBN 2235-3151:86–99, 2020.

[2] Parenteau, C.S., Zuby, D., Brolin, K., Svensson, M.Y. et al., "Restrained male and female occupants in frontal crashes: are we different?," in: International Research Council on the Biomechanics of Injury (ed.), *2013 IRCOBI Conference Proceedings*, IRCOBI Conference Proceedings, IRCOBI Conference, Gothenburg, Sweden, 11.-13.9.2013, IRCOBI, 2013.

[3] Forman, J., Poplin, G.S., Shaw, C.G., McMurry, T.L. et al., "Automobile injury trends in the contemporary fleet: Belted occupants in frontal collisions," *Traffic Inj Prev* 20(6):607–612, 2019, doi:10.1080/15389588.2019.1630825.

[4] Abrams, M.Z. and Bass, C.R., "Female vs. Male relative fatality risk in fatal crashes," in: International Research Council on the Biomechanics of Injury (ed.), *2020 IRCOBI Conference Proceedings*, IRCOBI Conference Proceedings, IRCOBI Conference, postponed (online), IRCOBI, ISBN 2235-3151:47–85, 2020.

[5] Nutbeam, T., Weekes, L., Heidari, S., Fenwick, R. et al., "Sex-disaggregated analysis of the injury patterns, outcome data and trapped status of major trauma patients injured in motor vehicle collisions: a prespecified analysis of the UK trauma registry (TARN)," *BMJ Open* 12(5):e061076, 2022, doi:10.1136/bmjopen-2022-061076.

[6] Brumbelow, M.L. and Jermakian, J.S., "Injury risks and crashworthiness benefits for females and males: Which differences are physiological?," *Traffic Inj Prev* 23(1):11–16, 2022, doi:10.1080/15389588.2021.2004312.

[7] Leo, C., Rizzi, M.C., Bos, N.M., Davidse, R.J. et al., "Are There Any Significant Differences in Terms of Age and Sex in Pedestrian and Cyclist Accidents?," *Front. Bioeng. Biotechnol.* 9, 2021, doi:10.3389/fbioe.2021.677952.

[8] Linder, A. and Svedberg, W., "Review of average sized male and female occupant models in European regulatory safety assessment tests and European laws: Gaps and bridging suggestions," *Accident Analysis & Prevention* 127:156–162, 2019, doi:10.1016/j.aap.2019.02.030.

[9] Schneider, L.W., Robbins, D.H., Pflüg, M.A., and Snyder, R.G., "Development of anthropometrically based design specifications for an advanced adult anthropomorphic dummy family, volume 1.: Final Report. UMTRI-83-53.," Technical Report UMTRI-83-53-1, 1983.

[10] John, J., Klug, C., Kranjec, M., Svenning, E. et al., "Hello, world! VIVA+: A human body model lineup to evaluate sex-differences in crash protection," *Frontiers in bioengineering and biotechnology* 10, 2022, doi:10.3389/fbioe.2022.918904.

[11] Schubert, A., Erlinger, N., Leo, C., Iraeus, J. et al., "Development of a 50th Percentile Female Femur Model," in: International Research Council on the Biomechanics of Injury (ed.), *2021 IRCOBI Conference Proceedings*, IRCOBI Conference Proceedings, IRCOBI Conference, Munich, Germany, IRCOBI:308-332, 2021.

[12] John, J., Putra, I.P.A., and Iraeus, J., "Finite Element Human Body Models to study Sex-differences in Whiplash Injury: Validation of VIVA+ passive response in rear-impact," in: International Research Council on the Biomechanics of Injury (ed.), *2022 IRCOBI Conference Proceedings*, IRCOBI Conference Proceedings, IRCOBI Conference, Porto, Portugal, 14.-16.9., IRCOBI, ISBN 2235-3151:215–227, 2022.

[13] Iraeus, J. and Lindquist, M., "Development and validation of a generic finite element vehicle buck model for the analysis of driver rib fractures in real life nearside oblique frontal crashes," *Accident Analysis & Prevention* 95(Pt A):42–56, 2016, doi:10.1016/j.aap.2016.06.020.

[14] Park, J., Ebert, S.M., Reed, M.P., and Hallman, J.J., "Statistical Models for Predicting Automobile Driving Postures for Men and Women Including Effects of Age," *Human factors* 58(2):261–278, 2016, doi:10.1177/0018720815610249.
[15] Höschele, P., Smit, S., Tomasch, E., Östling, M. et al., "Generic Crash Pulses Representing Future Accident Scenarios of Highly Automated Vehicles," *SAE Int. J. Trans. Safety* 10(2), 2022, doi:10.4271/09-10-02-0010.
[16] Pipkorn, B., Iraeus, J., Björklund, M., Bunketorp, O. et al., "Multi-Scale Validation of a Rib Fracture Prediction Method for Human Body Models," in: International Research Council on the Biomechanics of Injury (ed.), *2019 IRCOBI Conference Proceedings*, IRCOBI Conference Proceedings, IRCOBI Conference, Florence, Italy, 11.-13.9., IRCOBI, ISBN 2235-3151:175–192, 2019.
[17] Lawrence, J.M. and Siegmund, G.P., "Seat back and head restraint response during low-speed rear-end automobile collisions," *Accident Analysis & Prevention* 32(2):219–232, 2000, doi:10.1016/s0001-4575(99)00108-6.
[18] Svensson, M.Y., Boström, O., Davidsson, J., Hansson, H.-A. et al., "Neck injuries in car collisions — a review covering a possible injury mechanism and the development of a new rear-impact dummy," *Accident Analysis & Prevention* 32(2):167–175, 2000, doi:10.1016/s0001-4575(99)00080-9.
[19] Kitagawa, Y., Yamada, K., Motojima, H., and Yasuki, T., "Consideration on Gender Difference of Whiplash Associated Disorder in Low Speed Rear Impact," in: International Research Council on the Biomechanics of Injury (ed.), *2015 IRCOBI Conference Proceedings*, IRCOBI Conference Proceedings, IRCOBI Conference, Lyon, France, 9.-11.9.2015, IRCOBI, ISBN 2235-3151:233–245, 2015.
[20] Schmitt, K.-U., Weber, T., Svensson, M., Davidsson, J. et al., "Seat testing to investigate the female neck injury risk – preliminary results using a new female dummy prototype," in: International Research Council on the Biomechanics of Injury (ed.), *2012 IRCOBI Conference Proceedings*, IRCOBI Conference Proceedings, IRCOBI Conference, Dublin, Ireland, 12.-14.09.2012, IRCOBI:263, 2012.
[21] Mertz, H.J., Prasad, P., and Nusholtz, G., "Head Injury Risk Assessment for Forehead Impacts," in: SAE International (ed.), *International Congress & Exposition*, SAE Technical Paper Series, vol. 960099, International Congress & Exposition, 26.2.1996, SAE International, 1996.
[22] Gabler, L.F., Crandall, J.R., and Panzer, M.B., "Development of a Second-Order System for Rapid Estimation of Maximum Brain Strain," *Ann Biomed Eng* 47(9):1971–1981, 2019, doi:10.1007/s10439-018-02179-9.
[23] Wu, T., Sato, F., Antona-Makoshi, J., Gabler, L.F. et al., "Integrating Human and Nonhuman Primate Data to Estimate Human Tolerances for Traumatic Brain Injury," *J Biomech Eng* 144(7), 2022, doi:10.1115/1.4053209.
[24] Euro NCAP, Technical Bulletin, "Brain Injury Calculation," TB0 35, 1st ed., Rev. Feb. 2022.
[25] Larsson, K.-J., Blennow, A., Iraeus, J., Pipkorn, B. et al., "Rib Cortical Bone Fracture Risk as a Function of Age and Rib Strain: Updated Injury Prediction Using Finite Element Human Body Models," *Frontiers in bioengineering and biotechnology* 9:677768, 2021, doi:10.3389/fbioe.2021.677768.
[26] Forman, J.L., Kent, R.W., Mroz, K., Pipkorn, B. et al., "Predicting Rib Fracture Risk with Whole-Body Finite Element Models: Development and Preliminary Evaluation of a Probabilistic Analytical Framework," *Annals of Advances in Automotive Medicine* 56:109–124, 2012.
[27] Kullgren, A., Eriksson, L., Boström, O., and Krafft, M., "Validation of neck injury criteria using reconstructed real-life rear-end crashes with recorded crash pulses," *Proc. Int. Tech. Conf. Enhanced Safety Vehicles* 2003:13 -13 p, 2003.
[28] Eriksson, L. and Kullgren, A., "Influence of seat geometry and seating posture on NIC(max) long-term AIS 1 neck injury predictability," *Traffic injury prevention* 7(1):61–69, 2006, doi:10.1080/15389580500413000.
[29] Ola Boström, Mats Y Svensson, Bertil Aldman, Hans Arne Hansson et al., "A new neck injury criterion candidate-based on injury findings in the cervical spinal ganglia after experimental neck extension trauma," in: International Research Council on the Biomechanics of Injury (ed.), *1996 IRCOBI Conference Proceedings*, IRCOBI Conference Proceedings, IRCOBI Conference, Dublin, Ireland, 11. - 13. September, IRCOBI:123-136, 1996.
[30] PIPER Project, "PIPER Project," http://www.piper-project.eu, May 2, 2022.
[31] Iraeus, J., "Stochastic finite element simulations of real life frontal crashes: With emphasis on chest injury mechanisms in near-side oblique loading conditions," Dissertation, Umeå, 2015.
[32] Feist, F., Sharma, N., Klug, C., Roth, F. et al., "GVTR: A Generic Vehicle Test Rig Representative of the Contemporary European Vehicle Fleet," in: NHTSA (ed.), *The 26th ESV Conference Proceedings*, ESV Conference Proceedings, International Technical Conference on the Enhanced Safety of Vehicles, Eindhoven, Netherlands, 10-13 June, 2019.
[33] Alvarez, V.S. and Kleiven, S., "Importance of Windscreen Modelling Approach for Head Injury Prediction," in: International Research Council on the Biomechanics of Injury (ed.), *2016 IRCOBI Conference Proceedings*, IRCOBI Conference Proceedings, IRCOBI Conference, Malaga, Spain, 14.-16.9.2016, IRCOBI, ISBN 2235-3151:813–830, 2016.
[34] Pyttel, T., Liebertz, H., and Cai, J., "Failure criterion for laminated glass under impact loading and its application in finite element simulation," *International Journal of Impact Engineering* 38(4):252–263, 2011, doi:10.1016/j.ijimpeng.2010.10.035.

APPENDIX A – METHOD

The table below summarises the sources used for the calculation of the injury risks based on the respective injury metric.

Table A1. Injury risk curves and predictors used in the study

	Based on	Sources
HIC	Resultant Head CoG accelerations filtered with CFC1000	[21]
DAMAGE MPS	DAMAGE implementation in dynasaur using head rotation sensors implemented in VIVA+ definition files, filtered with CFC60.	[22] [23] [24]
Risk of 3+ fractured ribs	Risk per rib determined based on maximum strain per rib. Combined to overall risk of 3+ fractured ribs using probabilistic method.	[25] [26]
Proximal femur fracture risk	Risk based on MPS99 using risk curves calibrated for VIVA+ model	[11]
Femur shaft fracture risk	Risk based on MPS99 using risk curves calibrated for VIVA + model	[11]
NIC	Based on Head and T1 CoG acceleration from VIVA+ sensor (constrained with *CONSTRAINED_INTERPOLATION), filtered with CFC60 using Dynasaur	[27] [28] [29]

The python library dynasaur[2] was used for post-processing with the definition files that are part of the VIVA+ repository https://openvt.eu/fem/viva/vivaplus/-/tree/main/model/postprocess/Dynasaur.

A1 Frontal and Near-Side Crashes in GVI

To account for the position of the pedals and the steering wheel, the initial posture was updated based on an occupant posture regression model [14].
Measurements from the initial setup in the GVI were taken and used as input for the regression model of the 50M occupant. The seat height parameter in the regression model for the 50F occupant was subsequently adjusted until the same eye level as for the 50M was achieved. Based on this regression model and the anthropometry data of the two HBMs, target coordinates for eight landmarks were derived. These were used to define a simple skeleton which was used as a reference to derive targets for the positioning simulation (marionette method), using the PIPER software [30]. The landmarks between the hip and the head were very consistent with the prediction for the 50M model and hence left unchanged. Figure A1 shows the predicted and the achieved 50M posture. For the 50F, the regression model prediction differed significantly for landmarks in the spine. Hence, the 50F torso posture was adjusted accordingly. Figure A2 illustrates the predicted and the achieved 50F posture.

The generic seatbelt was fitted to the HBM assuming the same D-ring position (as both models were positioned in the GVI with the same eye level). The belt system features a retractor pretensioner with a single stage load limiter at the shoulder belt side. The belt buckle slip ring is attached to the seat and of a conventional type, i.e. allowing belt slippage in both directions (no locking tongue). The other end of the belt, the anchor side, is attached to the seat base (i.e. also moving with the seat's longitudinal and height adjustments for the two anthropometries). For more details on the belt modelling itself, the reader is referred to the original publication of the GVI [13].

[2] https://gitlab.com/VSI-TUGraz/Dynasaur

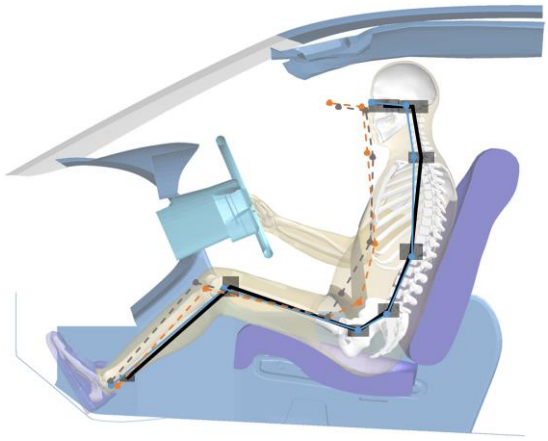

Figure A1. Comparison of model postures based on the regression model by Park et al. (2016) with the 50M model. The black bold lines indicate the posture prediction with the regression model for the 50M occupant. The grey boxes indicate the root mean squared error for each landmark position. The blue lines illustrate the actual posture achieved with the 50M in the generic vehicle interior shown in the background. The dashed lines indicate the predicted and achieved posture for the 50F model.

Figure A2. Comparison of model postures based on the regression model by Park et al. (2016) with the 50F model. The orange dashed lines illustrate the posture achieved for the 50F model. As a reference, the posture prediction for the 50F occupant is shown in dashed grey lines. The torso of the 50F model was repositioned slightly from the initial posture in order to better match the predicted head position. Note that the regression model predicts a knee position which is not achievable with the femur length in the present model.

A1.1 Frontal Impacts

Two crash pulses were considered for the frontal impact: a full overlap frontal crash at 56 km/h (FF56) and an oblique load case with the host vehicle travelling at 53 km/h (impact angle: 4°) colliding with an opponent vehicle (impact angle -21°), which is travelling at 35 km/h (LTAPOD2_53_35_hl). Both are previously published generic crash pulses [15]. For the FF56, only longitudinal loads were considered. In the oblique case, in addition to the loading in x direction, also loading in y direction and rotations about the z-axis were applied. For a more complete perspective, the crash was also simulated in a mirrored configuration (i.e. host impact angle -4°, opponent impact angle 21°). To distinguish between these two configurations, they are referred to as oblique near side (ONS, host impact angle 4°) and oblique far side (OFS, host impact angle -4°). Figure A3 illustrates the acceleration time-histories of the selected crash loads and Figure A4 shows a plot of the rotational velocity about the z-axis for the oblique case.

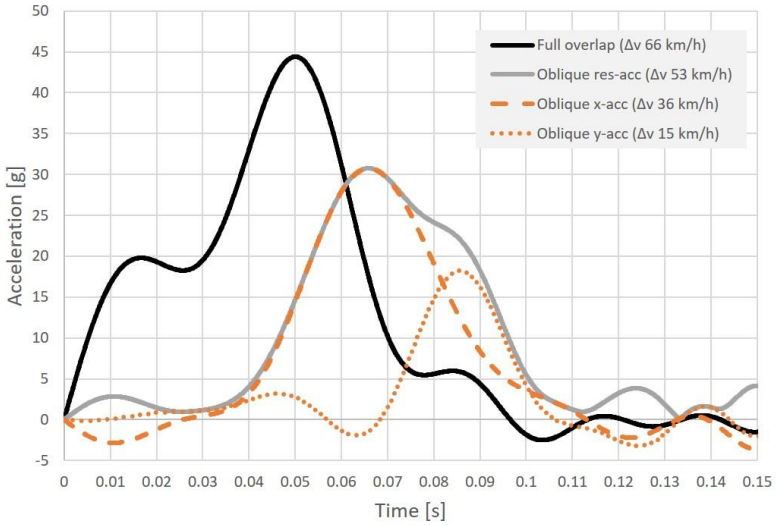

Figure A3. Time-history plot of the frontal crash loads. To simplify the illustration, all curves are shown with their maximum value in the positive direction. [15]

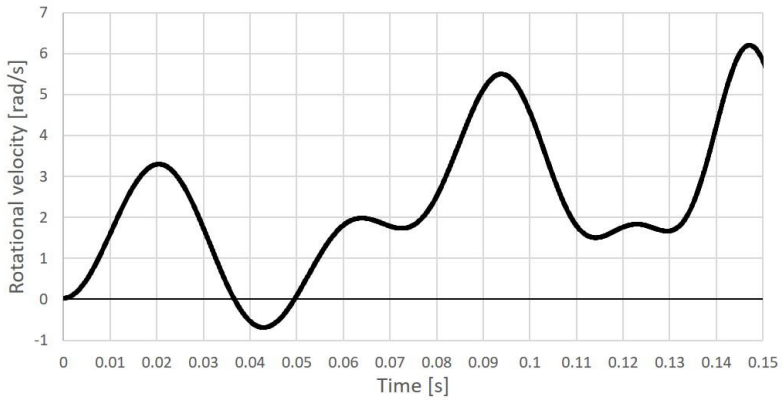

Figure A4. Time-history plot of the rotational velocity about the z-axis for the oblique case. [15]

To mimic different vehicles, three input parameters of the GVI were varied based on stochastic distributions [31]. Specifically, the stiffness of knee bolster, the shoulder belt force limiter level and the airbag pressure were varied. To avoid a large number of configurations with the seat belt and airbag compensating one another with their respective force/pressure levels, these two parameters were combined into three overall restraint system stiffness levels (i.e. they were not varied independently). Table A2 lists the resulting simulation matrix for the frontal load cases, which were performed for both occupant models.
The GVI model is available open-source at https://openvt.eu/fem/generic-vehicle-interior.

Table A2. Simulation matrix for the frontal and oblique load cases.

ID	Crash pulse	Knee force [kN]	Belt force [kN]	DAB pressure [bar]
001	FF56	5.59	3.25	1.21
002	FF56	5.59	3.94	1.31
003	FF56	5.59	4.63	1.41
004	FF56	9.45	3.25	1.21
005	FF56	9.45	3.94	1.31
006	FF56	9.45	4.63	1.41
007	FF56	13.31	3.25	1.21
008	FF56	13.31	3.94	1.31
009	FF56	13.31	4.63	1.41
010	Oblique near side	5.59	3.25	1.21
011	Oblique near side	5.59	3.94	1.31
012	Oblique near side	5.59	4.63	1.41
013	Oblique near side	9.45	3.25	1.21
014	Oblique near side	9.45	3.94	1.31
015	Oblique near side	9.45	4.63	1.41
016	Oblique near side	13.31	3.25	1.21
017	Oblique near side	13.31	3.94	1.31
018	Oblique near side	13.31	4.63	1.41
019	Oblique far side	5.59	3.25	1.21
020	Oblique far side	5.59	3.94	1.31
021	Oblique far side	5.59	4.63	1.41
022	Oblique far side	9.45	3.25	1.21
023	Oblique far side	9.45	3.94	1.31
024	Oblique far side	9.45	4.63	1.41
025	Oblique far side	13.31	3.25	1.21
026	Oblique far side	13.31	3.94	1.31
027	Oblique far side	13.31	4.63	1.41

A1.2 Side Impact

As with the frontal load cases, input parameters for the side impacts were varied to mimic different vehicles. The maximum intrusion into the GVI and the side airbag (SAB) pressure were selected for these simulations. In the GVI, lateral intrusions are applied by deforming the side structure towards the occupant by the distance determined by the desired maximum intrusion, scaled by individual horizontal (seven levels) and vertical (nine levels) scale factors. Hence, an intrusion pattern was derived by evaluating the results of 14 NCAP side impact pole crash tests available from the NHTSA's Vehicle Crash Test Database (https://www.nhtsa.gov/research-data/research-testing-databases#/vehicle). Table A3 lists the selected tests and their maximum intrusion at the five height levels recorded in the tests. Based on the maximum of these five values, a relative vertical intrusion pattern was derived for each test. These were very consistent across the tests (max. standard deviation 0.08). For use in the GVI, the mean at each level was calculated and these five values were directly used as input for the intrusion scaling at the GVI levels 1, 4, 5, 6, and 9 as they were deemed to be equivalent when comparing the measurement heights in the tests with the beam positions in the GVI. The remaining values for level 2, 3, 7, and 8 were derived from linear interpolation.

Table A3. Maximum intrusions from single vehicles from NHTSA's Vehicle Crash Test Database, which were used to derive deformation profile within the current study

		Crush at Level [in mm]				
Vehicle	**Test ID**	**1**	**2**	**3**	**4**	**5**
2020 Nissan Maxima S 4-Door Sedan	10960	416	425	433	335	149
2020 Hyundai Accent SE 4-Door Sedan	10969	249	289	303	284	108
2020 MAZDA3 4-Door Sedan	10973	256	264	261	256	58
2019 Audi A6 quattro 4-Door Sedan	10983	281	306	319	247	59
2020 Hyundai Sonata SE 4-Door Sedan	11050	268	320	331	290	71
2020 Nissan Sentra 4-Door Sedan	11069	248	285	297	257	108
2020 Cadillac CT5 Luxury 4-Door Sedan	11082	285	329	333	293	97
2021 Kia K5 LXS 4-Door Sedan	11269	310	329	344	288	67
2021 Acura TLX 4-Door Sedan	11353	260	290	305	228	48
2021 Lexus IS 300 4-Door Sedan	11385	335	374	386	313	85
2021 BMW 330i 4-Door Sedan Sedan	11498	265	308	326	278	62
2021 Hyundai Elantra SEL 4-Door Sedan	11577	248	280	288	274	103
2021 Genesis G80 4-Door Sedan	11619	254	313	335	299	109
2022 Honda Civic LX 4-Door Sedan	14050	249	287	295	244	38

For one test (No. 10983), the horizontal intrusion patterns at the five provided height levels were studied further. The difference between the post and pre-test measurements were compared to the maximum intrusion at each level (again yielding a relative intrusion pattern for each level). These relative intrusions patterns were also consistent across the height levels. Since the horizontal measurements were taken at 22 points but only 7 can be used as input in the GVI, the relative intrusion pattern was mapped to the positions of these points. While the measurements from the crash tests were taken based on the plastic exterior deformation, in the GVI, the intrusions are applied by moving and deforming the entire side structure towards the occupant. Hence, when using these measurements as input directly, the intrusions would be overestimated. To avoid this, the distances between the exterior and the interior (which would act as crumple zones acting in an actual crash) were estimated at each intrusion position from evaluating the FE model. This distance was then subtracted from the intrusion pattern resulting from the desired maximum intrusion combined with the seven horizontal and nine vertical intrusion scale factors.

Overall, two maximum intrusions (the mean and maximum intrusion observed in the crash tests) and three SAB pressure levels were used in the simulations.

Table A4 lists the resulting simulation matrix for the lateral load cases, which were performed for both occupant models.

Table A4. Simulation matrix for the lateral load cases.

ID	Max. intrusion level [mm]	SAB pressure [bar]
101	325.4	1.27
102	325.4	1.40
103	325.4	1.53
104	433.0	1.27
105	433.0	1.40
106	433.0	1.53

A2 VRU Crashes

A1.3 GVE Validation

The stiffness characteristics of spoiler, bumper and bonnet leading edge of the GVE models were compared to corridors from current fleet data from [32]. The results of the impactor tests can be seen in Table A5.

Table A5. Response of the impactor test (black) compared to the results reported in Feist et al. [32]

Oblique spoiler test (SPV)	Bumper impact, horizontal (BMP)	Bonnet leading egde impact, oblique (BLE)
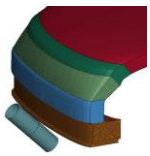	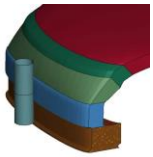	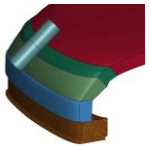
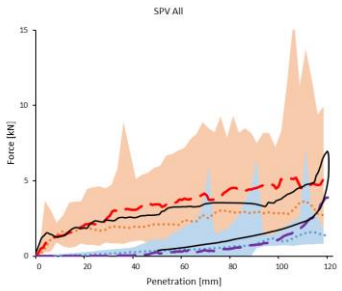	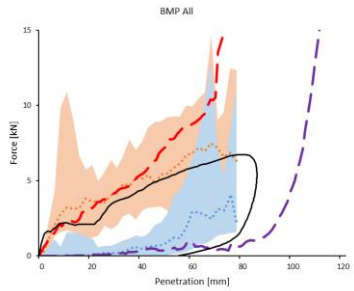	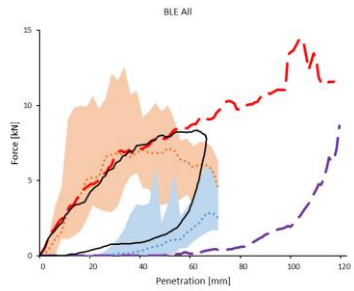
		

In the original GV models according to Euro NCAP Technical Bulletin TB024, the windscreen was modelled rigid. To enable a more realistic injury assessment, this was adjusted in the current study. The windscreen was modelled with a solid PVC layer coffered by two shell glass layers. With the help of a head impactor test on the outside of the windscreen the response of the windscreen was compared with the values reported in [33] for experiments performed by [34]. The impact velocity of the head impactor (mass: 4.58 kg) was adjusted to 10.24 m/s to achieve the same kinetic energy of 240 J as reported. The results of this comparison are shown in Figure A5.

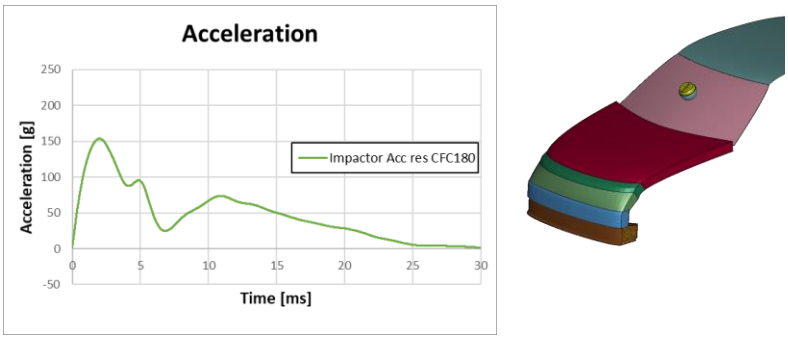

Figure A5. Impactor results with CFC180 filtered impactor acceleration (middle) and location of the head impactor impact on the windscreen (right). Results were compared with those presented Alvarez et al. [33]

A1.4 Bicyclist Models

For simulations with the average female bicyclist, a bicycle with trapeze frame (Figure A6) was used and for simulations with the average male bicyclist, a bicycle with diamond frame (Figure A7) was used.

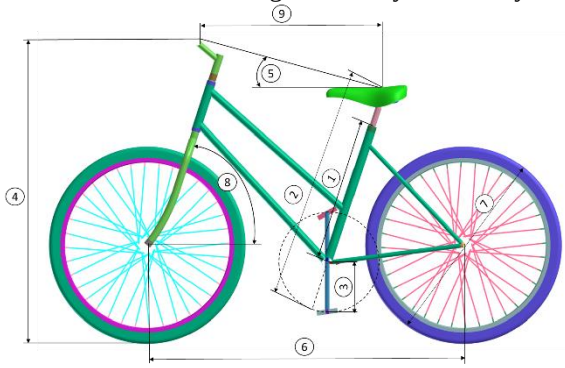

Figure A6. Trapeze Frame Bicycle for VIVA+ 50F simulations

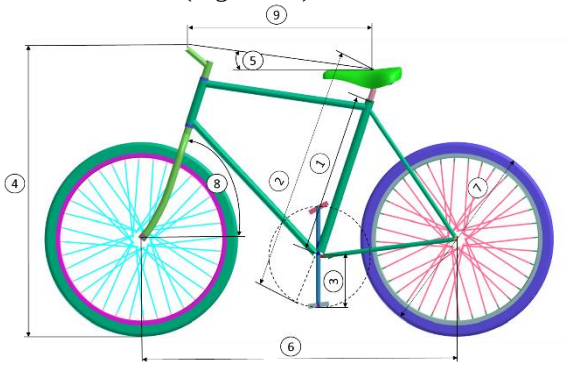

Figure A7. Diamond Frame Bicycle for VIVA+ 50M simulations

Both bicycle models can be found on the openVT platform. The dimensions of both bicycles are shown in Table A6 and Table A7.

Table A6. Target geometry for trapeze frame VIVA+ 50F

#	Measurement	Goal
1	Frame Size	480 mm
2	Saddle Height	790 mm
3	Crank Length	165 mm
4	Handlebar Height	1018 mm
5	Handlebar to Saddle Angle	14°
6	Wheelbase	1062 mm
7	Wheel Diameter	660 mm
8	Head Tube Angle	66.8°
9	Handlebar to Saddle Distance	650 mm
10	Weight	11.7 kg
11	Sitting inclination	68.0°

Table A7. Target geometry for diamond frame VIVA+ 50M

#	Measurement	Goal
1	Frame Size	550 mm
2	Saddle Height	840 mm
3	Crank Length	165 mm
4	Handlebar Height	966 mm
5	Handlebar to Saddle Angle	7°
6	Wheelbase	1077 mm
7	Wheel Diameter	660 mm
8	Head Tube Angle	66.7°
9	Handlebar to Saddle Distance	623 mm
10	Weight	11.3 kg
11	Sitting inclanation	70.0°

The cyclist was positioned according the values given in Figure A8 for the 50th percentile female and 50th percentile male. A stick figure where all the values are displayed is given in Figure A8. To achieve the inclantion given in Table A8, the 50th percentile female was rotated 22° forward about the y-axis and the 50th percentile male rotated 20° forward about the y-axis. The positioned VIVA+ 50F model can be seen in Figure A9 and the positioned VIVA+ 50M in Figure A10. These positioned models can be found on the openVT platform as part of the VIVA+ repository (https://openvt.eu/fem/viva/positioned-models/vivaplus-bicyclist).

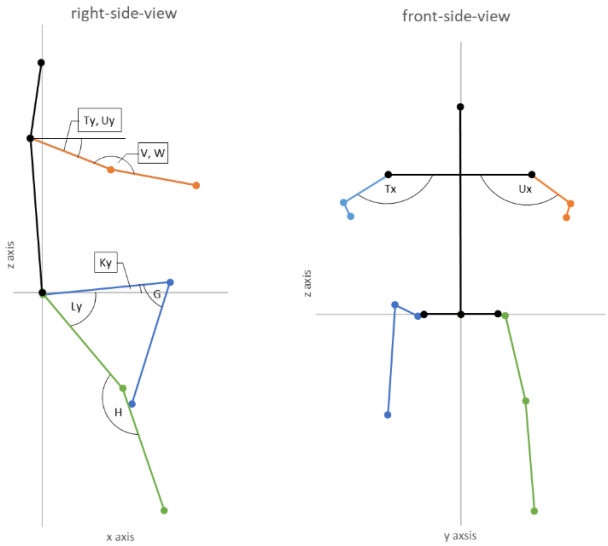

Figure A8. Reference Posture of 50F and 50M cyclist with left food down

Table A8. Reference Posture of 50F and 50M cyclist

Abbrev.	**Measure**	**50F L-Down**	**50M L-Down**
Px	Heel to heel distance longitudinal	99.627 mm	120.20 mm
Py	Heel to heel distance lateral	301.737 mm	299.60 mm
Pz	Heel to heel distance vertical	319.531 mm	321.5 mm
Ky	Right Upper Leg Angle (around Y w.r.t. horizontal)	4.93°	6.03°
Ly	Left Upper Leg Angle (around Y w.r.t. the horizontal)	52.03°	46.78°
G	Right Knee flexion Angle (Y)	68.77°	75.15°
H	Left Knee flexion Angle (Y)	145.52°	155.23°
Ty	Right Upper Arm Angle (Y w.r.t. horizontal)	22.67°	24.90°
Uy	Left Upper Arm Angle (Y w.r.t. horizontal	22.80°	24.51°
Tx	Right Upper Arm Angle (X w.r.t. horizontal)	135.27°	114.47°
Ux	Left Upper Arm Angle (X w.r.t. horizontal)	130.25°	116.50°
V	Right Elbow flexion Angle	168.29°	169.77°
W	Left Elbow flexion Angle	168.29°	169.61°
HCx	x-Position of HC relative to AC	-2.411 mm	9.80 mm

Figure A9. Positioned 50F cyclist model in front of GV sedan model

Figure A10. Positioned 50M cyclist model in front of GV sedan model

APPENDIX B – DETAILED SIMULATION RESULTS

B1 Frontal impacts

50F 50M

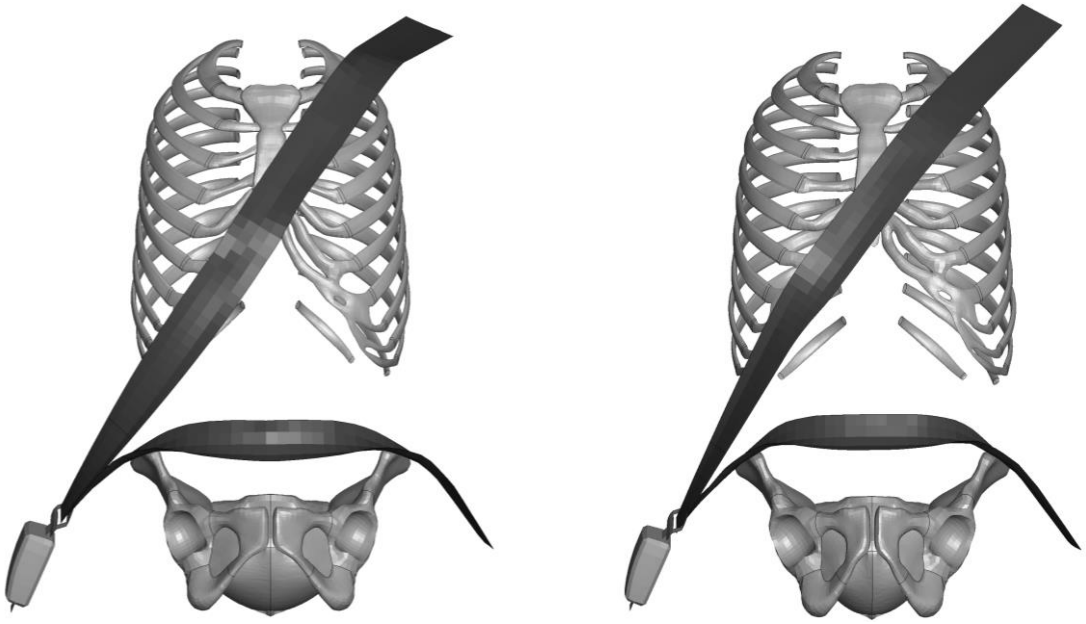

Figure B1. Initial position of 50F and 50M VIVA+ model (t0) in GVI.

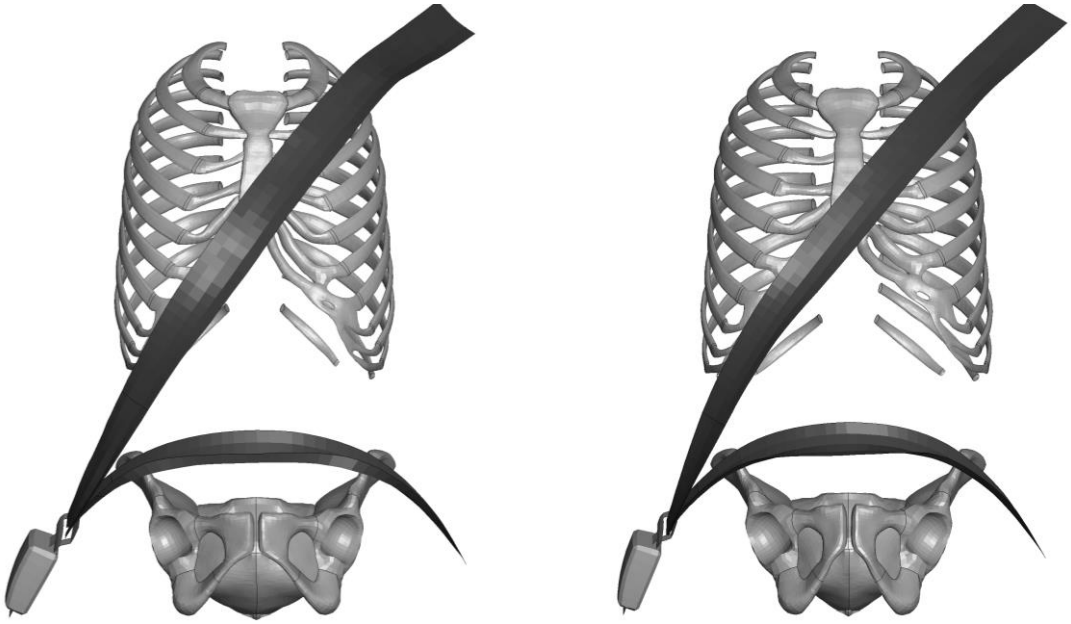

Figure B2. Initial position of 50F and 50M VIVA+ model at frontal impact after belt pre-tensioning (25 ms).

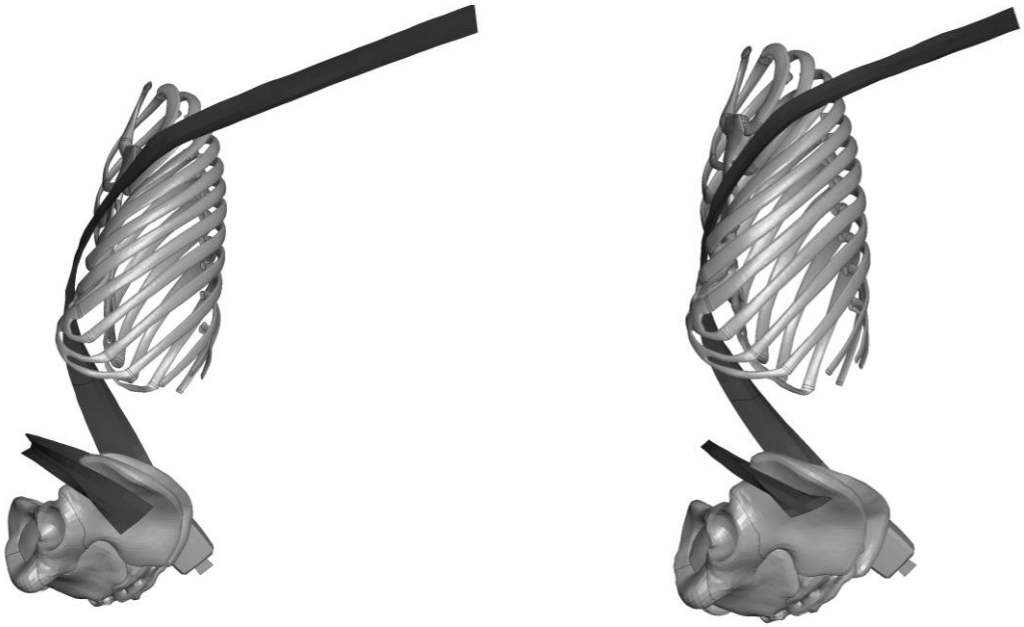

Figure B3. Belt-pelvis and belt-rib interaction in frontal impact (ID 003/203). Side view just before rebound is imitated for 50F (t=65 ms) and 50M (t=80 ms) VIVA+ .

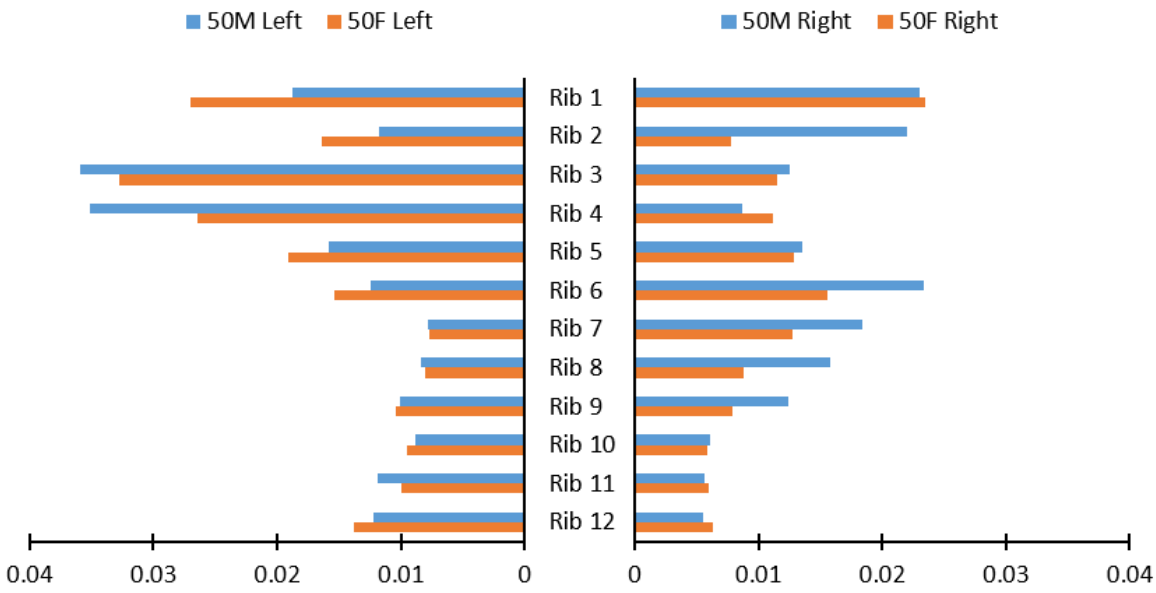

Figure B4. Maximum principal strain (MPS, max. integration point, tensile strains only) distribution in the ribs of the 50F compared to the 50M VIVA+ model in a simulated frontal crash (ID 003/203) for left and right side of the chest.

Table B1. Results of all simulated frontal/oblique impacts with the 50F and 50M VIVA+ models.

ID	Pulse	Knee bolster stiffn.	Shoulder belt limiter	Airbag pressure	VIVA+ model	HIC15 AIS3+ risk	DAMAGE AIS4+ risk	3+ fract. ribs risk (50 yo)	Left proximal femur fract. risk	Right proximal femur fract. risk	Left femur shaft fract. risk	Right femur shaft fract. risk
001	FF56	soft	soft	soft	50M	31.38%	25.69%	91.40%	10.30%	9.89%	0.36%	0.11%
002	FF56	soft	median	median	50M	3.65%	34.39%	72.28%	8.80%	9.15%	0.21%	0.10%
003	FF56	soft	stiff	stiff	50M	4.68%	60.50%	66.79%	8.13%	7.80%	0.15%	0.10%
004	FF56	median	soft	soft	50M	29.66%	33.96%	91.19%	22.52%	12.70%	0.99%	0.16%
005	FF56	median	median	median	50M	3.24%	38.49%	87.38%	14.24%	13.06%	0.47%	0.16%
006	FF56	median	stiff	stiff	50M	3.74%	58.59%	70.34%	11.99%	9.44%	0.32%	0.15%
007	FF56	stiff	soft	soft	50M	33.25%	30.35%	93.09%	36.48%	17.07%	1.77%	0.20%
008	FF56	stiff	median	median	50M	2.91%	46.74%	87.98%	24.56%	13.65%	0.90%	0.19%
009	FF56	stiff	stiff	stiff	50M	3.19%	61.67%	77.68%	18.47%	9.83%	0.51%	0.18%
010	ONS	soft	soft	soft	50M	0.02%	0.02%	69.02%	4.38%	5.08%	0.11%	0.05%
011	ONS	soft	median	median	50M	0.02%	0.03%	81.43%	4.36%	6.37%	0.07%	0.05%
012	ONS	soft	stiff	stiff	50M	0.02%	0.31%	98.73%	3.60%	8.05%	0.05%	0.07%
013	ONS	median	soft	soft	50M	0.01%	0.01%	69.50%	7.82%	6.65%	0.14%	0.07%
014	ONS	median	median	median	50M	0.02%	0.05%	76.99%	7.44%	6.86%	0.13%	0.07%
015	ONS	median	stiff	stiff	50M	0.01%	0.33%	95.74%	7.17%	8.64%	0.14%	0.07%
016	ONS	stiff	soft	soft	50M	0.01%	0.02%	52.69%	11.05%	6.40%	0.20%	0.08%
017	ONS	stiff	median	median	50M	0.03%	0.08%	74.52%	10.71%	6.99%	0.16%	0.09%
018	ONS	stiff	stiff	stiff	50M	0.02%	1.00%	97.45%	9.14%	9.45%	0.15%	0.09%
019	OFS	soft	soft	soft	50M	0.48%	0.45%	18.88%	12.99%	3.41%	0.10%	0.34%
020	OFS	soft	median	median	50M	1.02%	0.23%	19.98%	17.80%	2.98%	0.16%	0.36%
021	OFS	soft	stiff	stiff	50M	3.16%	0.18%	23.81%	16.74%	2.96%	0.12%	0.36%
022	OFS	median	soft	soft	50M	2.40%	1.29%	11.89%	15.27%	3.20%	0.14%	0.37%
023	OFS	median	median	median	50M	0.99%	0.51%	18.81%	20.80%	3.22%	0.14%	0.36%
024	OFS	median	stiff	stiff	50M	2.03%	0.35%	24.94%	16.68%	2.76%	0.14%	0.37%
025	OFS	stiff	soft	soft	50M	0.52%	0.93%	12.36%	17.99%	3.25%	0.21%	0.39%
026	OFS	stiff	median	median	50M	1.18%	0.55%	21.21%	20.30%	3.80%	0.20%	0.39%

027	OFS	stiff	stiff	stiff	50M	5.11%	0.60%	22.58%	14.58%	2.63%	0.20%	0.35%
201	FF56	soft	soft	soft	50F	1.23%	21.92%	18.51%	7.99%	2.05%	0.18%	0.17%
202	FF56	soft	median	median	50F	2.84%	19.37%	29.08%	7.69%	1.47%	0.17%	0.17%
203	FF56	soft	stiff	stiff	50F	5.97%	3.13%	48.15%	5.99%	1.21%	0.16%	0.17%
204	FF56	median	soft	soft	50F	1.39%	28.46%	42.73%	39.11%	4.43%	0.43%	0.30%
205	FF56	median	median	median	50F	1.94%	14.35%	51.30%	25.76%	2.91%	0.43%	0.28%
206	FF56	median	stiff	stiff	50F	3.61%	11.44%	51.69%	22.83%	2.16%	0.43%	0.28%
207	FF56	stiff	soft	soft	50F	2.02%	20.58%	17.98%	68.07%	6.07%	0.66%	0.42%
208	FF56	stiff	median	median	50F	2.43%	12.11%	48.60%	44.44%	3.79%	0.64%	0.36%
209	FF56	stiff	stiff	stiff	50F	4.08%	4.08%	54.80%	40.22%	3.49%	0.66%	0.35%
210	ONS	soft	soft	soft	50F	0.09%	0.80%	41.10%	4.24%	5.44%	0.45%	0.20%
211	ONS	soft	median	median	50F	0.36%	1.53%	99.82%	7.27%	3.71%	0.58%	0.25%
212	ONS	soft	stiff	stiff	50F	0.51%	1.97%	99.06%	9.42%	5.33%	0.45%	0.34%
213	ONS	median	soft	soft	50F	0.05%	1.52%	35.76%	7.57%	5.57%	1.08%	0.50%
214	ONS	median	median	median	50F	0.24%	1.02%	99.03%	11.29%	6.83%	1.36%	0.63%
215	ONS	median	stiff	stiff	50F	0.33%	2.45%	97.07%	17.26%	5.71%	1.44%	0.77%
216	ONS	stiff	soft	soft	50F	0.06%	1.32%	50.56%	12.53%	6.18%	1.56%	0.73%
217	ONS	stiff	median	median	50F	0.20%	1.67%	99.22%	14.99%	5.87%	2.23%	0.94%
218	ONS	stiff	stiff	stiff	50F	0.22%	2.18%	91.27%	21.47%	6.73%	2.38%	1.15%
219	OFS	soft	soft	soft	50F	0.74%	0.65%	3.59%	12.79%	14.52%	0.23%	0.53%
220	OFS	soft	median	median	50F	0.00%	2.69%	2.68%	12.86%	17.88%	0.31%	0.60%
221	OFS	soft	stiff	stiff	50F	0.01%	4.00%	3.08%	11.45%	26.85%	0.41%	0.73%
222	OFS	median	soft	soft	50F	0.91%	1.21%	2.98%	12.23%	32.27%	0.56%	1.07%
223	OFS	median	median	median	50F	0.00%	3.67%	2.60%	24.16%	37.63%	0.64%	1.08%
224	OFS	median	stiff	stiff	50F	0.00%	6.85%	2.69%	15.63%	68.37%	0.81%	1.34%
225	OFS	stiff	soft	soft	50F	0.98%	1.13%	2.20%	16.06%	38.57%	0.83%	1.49%
226	OFS	stiff	median	median	50F	0.00%	3.06%	5.01%	17.04%	48.63%	0.92%	1.77%
227	OFS	stiff	stiff	stiff	50F	0.00%	7.80%	1.45%	20.46%	65.90%	1.20%	2.30%

B2 Near-Side impacts

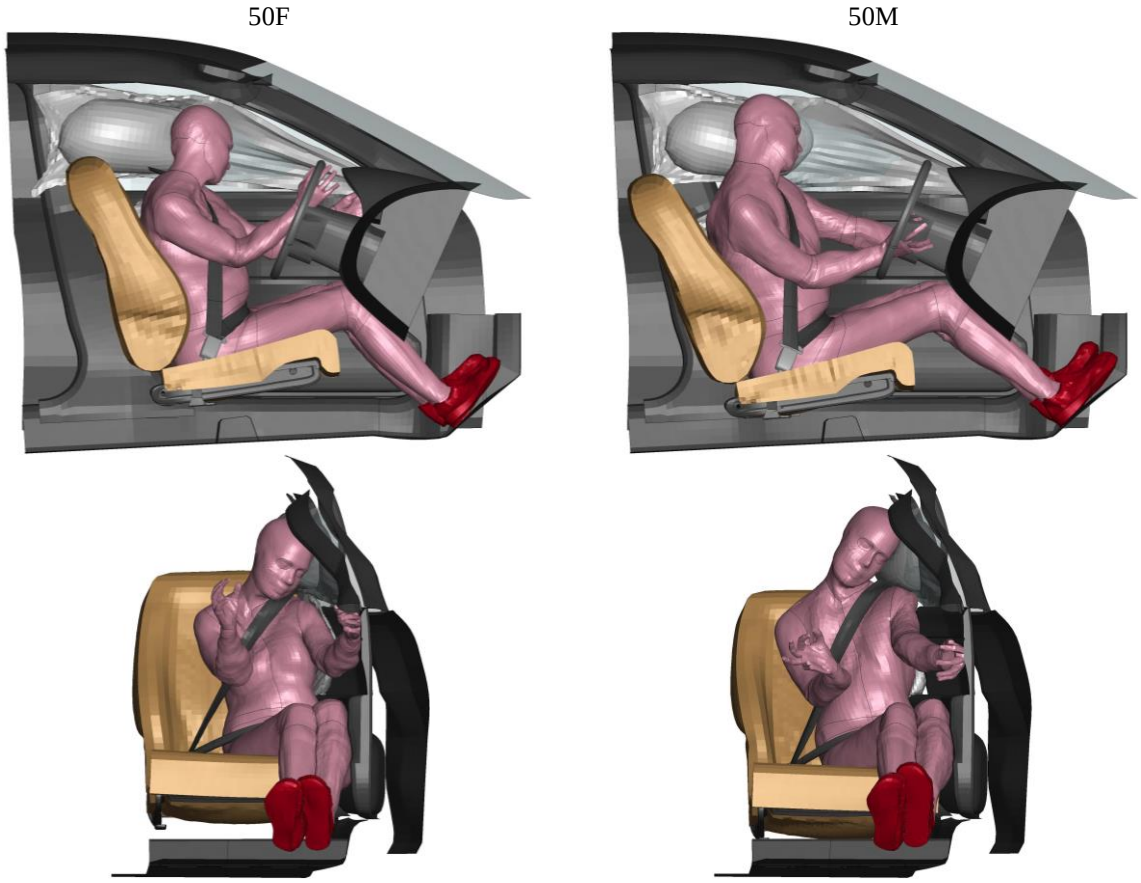

Figure B5. Animated results of near-side impacts with 50F and 50M VIVA+ models (ID 5) in GVI interacting with generic side airbags 70 ms into the simulation.

Figure B6. Overlay of 50F (red) and 50M (blue) VIVA+ model response for near-side impact (ID 5) 70 ms into the simulation.

Table B2. Results of all simulated lateral impacts with the 50F and 50M VIVA+ models.

ID	Intrusion	Airbag pressure	VIVA+	HIC15 AIS3+ risk	DAMAGE AIS4+ risk	3+ fract. ribs risk (50 yo)	Left proximal femur fract. risk	Right proximal femur fract. risk	Left femur shaft fract. risk	Right femur shaft fract. risk
101	mean	soft	50M	1.92%	38.37%	30.19%	2.03%	7.25%	0.43%	0.83%
102	mean	median	50M	1.84%	27.38%	29.99%	2.06%	7.35%	0.45%	0.92%
103	mean	stiff	50M	1.47%	22.86%	34.02%	2.10%	7.47%	0.44%	0.86%
104	max	soft	50M	3.55%	36.56%	52.72%	8.27%	6.82%	0.84%	0.37%
105	max	median	50M	3.19%	35.99%	7.87%	8.05%	7.17%	0.84%	0.37%
106	max	stiff	50M	3.21%	35.35%	7.93%	8.61%	8.00%	0.84%	0.36%
301	mean	soft	50F	12.72%	7.42%	20.63%	0.71%	1.11%	0.23%	0.18%
302	mean	median	50F	9.01%	20.68%	15.83%	0.74%	1.12%	0.26%	0.17%
303	mean	stiff	50F	8.60%	12.88%	25.62%	0.64%	1.19%	0.26%	0.18%
304	max	soft	50F	9.35%	2.42%	49.50%	4.61%	2.29%	0.43%	0.23%
305	max	median	50F	8.91%	5.06%	46.14%	5.16%	2.01%	0.44%	0.22%
306	max	stiff	50F	7.46%	2.88%	28.14%	3.92%	2.21%	0.50%	0.22%

B3 Rear-end impacts

Table B3. Simulation results with 50M and 50F VIVA+ models in Forvia innovative seat.

	50M	50F
Upper-most HR	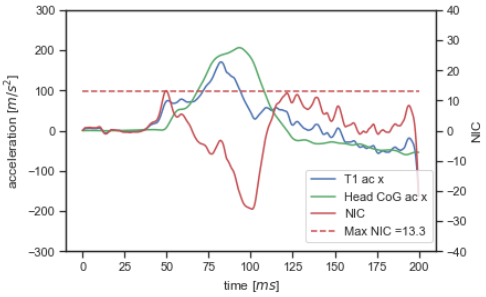	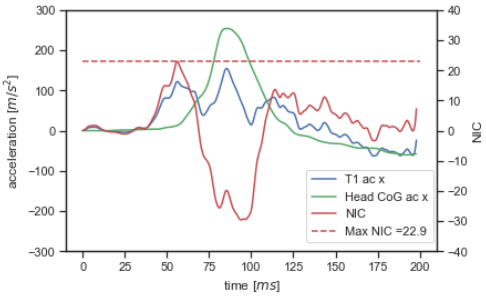
	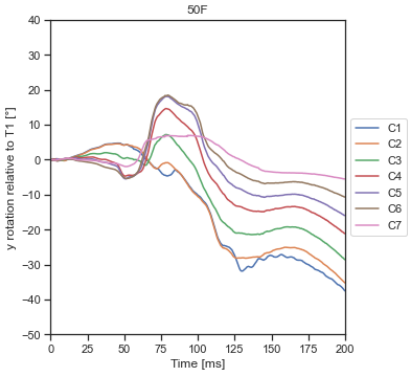	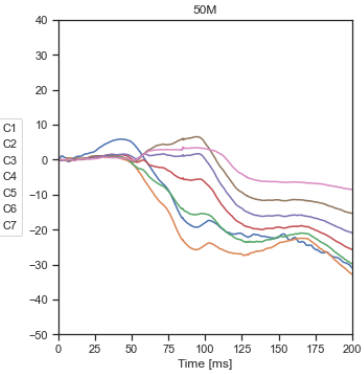
Mid HR	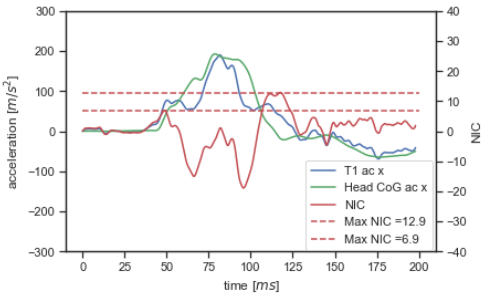	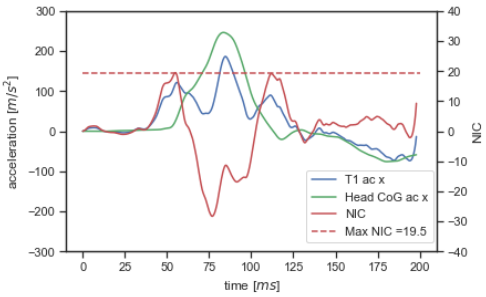
	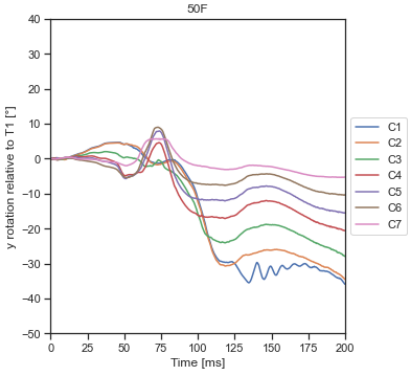	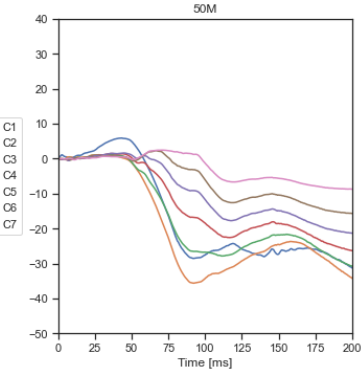

Lower-most HR

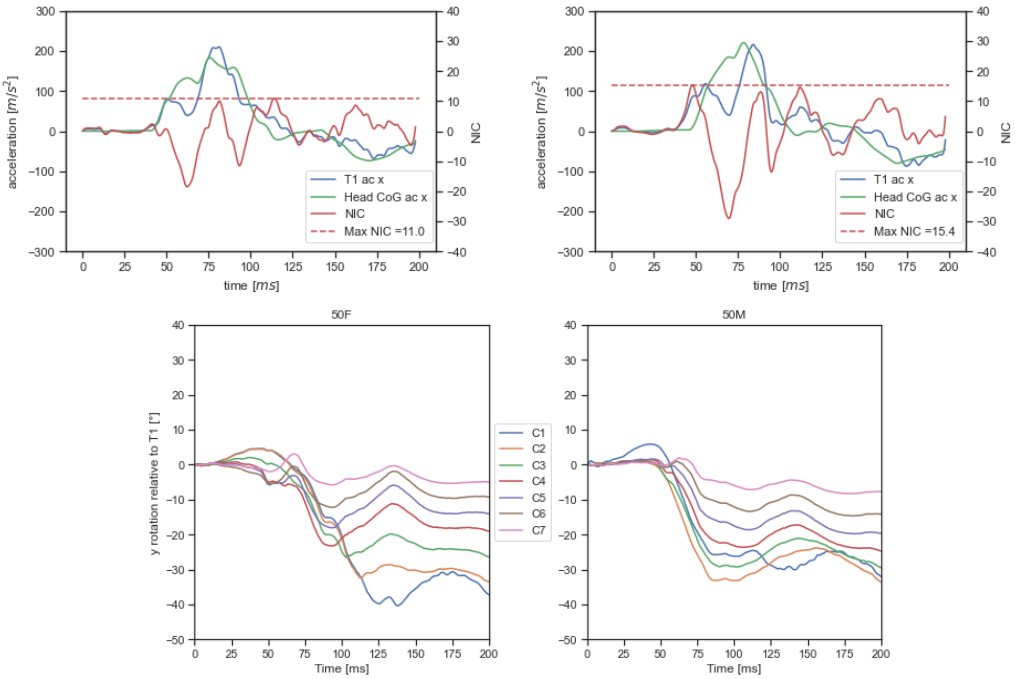

B4 Pedestrian impacts

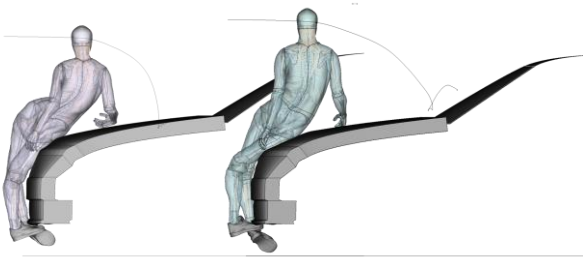

Figure B7. Pedestrian simulations with the VIVA+ 50F (left) and 50M (right) model, impacted by the GVE at the time of impact of the proximal femur on the bonnet leading edge. Additionally, the head trajectory and head impact location are visualised.

Table B4. Results of pedestrian simulations (struck side is highlighted in bold for the femur)

Car v [km/h]	Coll. Angle [°]	Vehicle Shape	VIVA+	HIC15 AIS3+ risk	DAMAGE AIS4+ risk	3+ fract. ribs risk (50 yo)	Left prox. femur fract. risk	Right prox. femur fract. risk	Left femur shaft fract. risk	Right femur shaft fract. risk
40	270	Sedan	50F	48.2%	50%	20.29	10%	**98.6%**	3.2%	**68.8%**
40	270	Sedan	50M	76.8%	95.6%	8.2%	57.6%	**6%**	0.9%	**65%**
40	90	Sedan	50F	88.2%	99.8%	0.0%	**88.8%**	26.9%	**44.2%**	1.5%
40	90	Sedan	50M	94.9%	54.5%	46.7%	**12.6%**	15.4%	**59.5%**	1%
40	270	SUV	50F	93.9%	100 %	96.6%	58.7%	**99.5%**	6%	**1.%**
40	270	SUV	50M	90.3%	82.7%	27.2%	12.1%	**100%**	4.2%	**12.5%**
40	90	SUV	50F	96.7%	100 %	85.7%	**97%**	67.4%	**0.7%**	6%
40	90	SUV	50M	97.2%	100%	62.8%	**100%**	27.4%	**6.8%**	10.8%

B5 Cyclist impacts

Table B5. Results of cyclist simulations (struck side is highlighted in bold for the femur)

Car v [km/h]	Coll. Angle [°]	Vehicle Shape	VIVA+	HIC15 AIS3+ risk	DAMAGE AIS4+ risk	3+ fract. ribs risk (50 yo)	Left prox. femur fract. risk	Right prox. femur fract. risk	Left femur shaft fract. risk	Right femur shaft fract. risk
40	270	Sedan	50F	94.6%	99.9%	99.5%	**12.7%**	25.6%	**100%**	0.4%
40	270	Sedan	50M	80.3%	9.5%	100%	**16.1%**	24.8%	**86.8%**	0.8%
40	90	Sedan	50F	91.4%	97.8%	68.6%	38%	**61.6%**	0.7%	**5.7%**
40	90	Sedan	50M	93.9%	30.8%	99.9%	92.2%	**25.7%**	3.1%	**0.7%**
40	270	SUV	50F	58.9%	100%	62.2%	**100%**	35.5%	**85.1%**	0.4%
40	270	SUV	50M	67.1%	84.2%	46.2%	**86.3%**	10.7%	**96.6%**	1.4%
40	90	SUV	50F	46.4%	100%	39.1%	10.4%	**42.7%**	23.4%	**5.2%**
40	90	SUV	50M	98.7%	57.2%	16.3%	100%	**27.7%**	58.8%	**1.9%**